



Fano resonances in nested wire media

David E. Fernandes,^{1,*} Stanislav I. Maslovski,^{1,†} George W. Hanson,^{2,‡} and Mário G. Silveirinha^{1,§}

¹*University of Coimbra, Department of Electrical Engineering–Instituto de Telecomunicações, 3030-290, Coimbra, Portugal*

²*Department of Electrical Engineering, University of Wisconsin–Milwaukee, 3200 N. Cramer Street, Milwaukee, Wisconsin 53211, USA*

(Received 1 May 2013; revised manuscript received 9 July 2013; published 26 July 2013)

We study the interaction of electromagnetic waves with two nested parallel metallic wire arrays, such that the unit cell of the structure has two inequivalent parallel wires. We develop a formalism to solve scattering problems using effective medium methods and prove that the electromagnetic coupling of the two sets of wires may result in the emergence of sharp Fano resonances.

DOI: [10.1103/PhysRevB.88.045130](https://doi.org/10.1103/PhysRevB.88.045130)

PACS number(s): 42.70.Qs, 78.20.Ci, 41.20.Jb

I. INTRODUCTION

The uniaxial wire medium consists of a set of infinitely long wires oriented along the same axis and embedded in a dielectric medium.^{1,2} Nanowire materials have been recently in focus due to their unusual electromagnetic properties, namely the hyperbolic dispersion of the photonic states,³ which among other things can provide for a negative refraction of light.^{4,5} Moreover, this type of artificial medium is gaining an increasing importance because it has proven to be useful in many applications in the microwave through mid-terahertz frequency band.^{6–12}

The wire medium is well known for its nonlocal (spatially dispersive) response, even in the quasistatic limit.^{13,14} Several modifications of the classical wire medium configuration (e.g., the periodic insertion of metallic plates in the metallic wires) that aim to reduce the spatially dispersive effects have been proposed¹⁵ and developed further in Refs. 16–19. The homogenization of double and triple perpendicular arrays of connected and nonconnected wire media has also been discussed in the literature.^{20–24} In particular, it has been shown that double-wire media may support highly confined interlaced plasmons.^{11,21}

Even though wire media formed by two nonconnected perpendicular wire arrays has been studied previously,²¹ the case wherein the two wire arrays are parallel, so that each unit cell of the material contains two parallel wires, remains an open problem. The solution of this problem is not trivial because the interaction between the nested wire arrays leads to the hybridization of the modes supported by the individual arrays, and in particular, the number of natural modes (plane waves) supported by the metamaterial (within an effective medium description) increases. We prove that if there is some structural asymmetry in the system (e.g., each subarray is made of a different metal or the subarrays are terminated differently at the interfaces), the electromagnetic coupling of the two subarrays may result in strong Fano-type resonances. The Fano resonance was originally discovered by Ugo Fano in his studies of autoionizing states of atoms,^{25,26} but because it results from the interference of two or more oscillators, it can in general be observed in quite distinct physical systems. In particular, Fano resonances have been recently demonstrated in plasmonic structures and metamaterials.^{26–29} Because of its narrow lineshape, Fano resonances have promising applications in sensing (e.g., in the development of novel chemical or biosensors). It should be mentioned that related wire media formed by triple

arrays of connected wires have been studied in Ref. 24, but in a different context; namely a drift-diffusion transport model was developed to characterize the electrodynamics of such media.

This paper is organized as follows. In Sec. II we propose an effective medium model for the bulk uniaxial wire medium formed by two nested sets of parallel wires. In Sec. III we introduce the boundary conditions required to solve the homogenization problem. In Sec. IV we present numerical calculations that validate our model and highlight the emergence of Fano resonances due to the interaction between the wire arrays. Finally, in Sec. V the conclusions are drawn.

II. EFFECTIVE PERMITTIVITY OF THE NESTED DOUBLE-WIRE MEDIUM

The standard wire medium is formed by a set of infinitely long metallic wires arranged in a periodic square lattice. Assuming that the wires are oriented along the z direction, it is known from previous studies^{13,14} that the wire medium is characterized by the effective permittivity tensor

$$\bar{\epsilon}_{\text{eff}}(\omega, k_z) = \epsilon_h \{ \epsilon_t (\hat{x}\hat{x} + \hat{y}\hat{y}) + \epsilon_{zz} \hat{z}\hat{z} \}, \quad (1)$$

where ϵ_h is the permittivity of the dielectric, $\epsilon_{zz} = 1 + [\frac{\epsilon_h}{(\epsilon_m - \epsilon_h)f_V} - \frac{\beta_h^2 - k_z^2}{k_p^2}]^{-1}$, $\beta_h = \omega\sqrt{\epsilon_h\mu_0}$ is the wave number in the dielectric host medium, $f_V = \pi(r/a)^2$ is the volume fraction of the metal, ϵ_m is the complex permittivity of the metallic wires, and k_p is a structural parameter with the physical meaning of plasma wave number. Within a thin wire approximation, we may state that $(k_p a)^2 \approx 2\pi [0.5275 + \ln(\frac{a}{2\pi R})]^{-1}$ and the transverse permittivity satisfies $\epsilon_t \approx 1$.^{13,14} The explicit dependence of the dielectric function on the wave vector $k_z \leftrightarrow -i\frac{d}{dz}$ implies a strong nonlocal behavior.^{13,14}

Here, we want to characterize the effective response of two nested sets of wires (denoted by A and B), such that the unit cell of the bulk material contains two metallic wires (Fig. 1). As discussed in Ref. 24, provided the two subarrays are not very strongly coupled in the near field, so that the influence of one array on the other can be regarded as a macroscopic excitation, the contribution of each array to the electric polarization is related to the macroscopic electric field as

$$\mathbf{P}_l = \left[\bar{\epsilon}_{\text{eff},l} \left(\omega, -i\frac{d}{dz} \right) - \epsilon_h \bar{\mathbf{I}} \right] \cdot \mathbf{E}, \quad l = A, B, \quad (2)$$

where $\bar{\epsilon}_{\text{eff},A}$ and $\bar{\epsilon}_{\text{eff},B}$ are defined as in Eq. (1), with pertinent structural parameters that depend on the considered subarray.

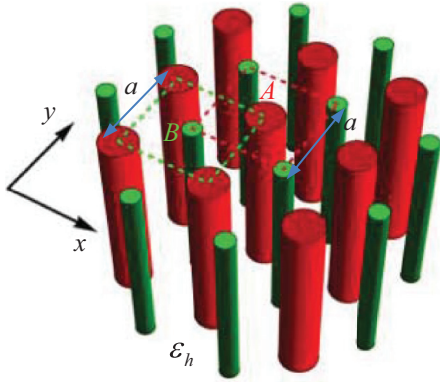


FIG. 1. (Color online) Geometry of the two nested wire media (denoted by A and B). The two arrays are arranged in a periodic square lattice with period a and the wires are embedded in a dielectric host material with permittivity ϵ_h .

The requirement that the two subarrays interact with one another as macroscopic sources is better satisfied if the two wires in the unit cell are as far apart as possible, which is the case represented in Fig. 1.

The effective dielectric function of the two nested arrays is supposed to describe the response of the total polarization vector $\mathbf{P}_A + \mathbf{P}_B$ to the macroscopic electric field. Thus, it must satisfy

$$\bar{\epsilon}_{\text{eff},A+B}(\omega, k_z) = \bar{\epsilon}_{\text{eff},A}(\omega, k_z) + \bar{\epsilon}_{\text{eff},B}(\omega, k_z) - \epsilon_h \bar{\mathbf{1}}. \quad (3)$$

This permittivity tensor is also of the form of Eq. (1) with the following zz component:

$$\epsilon_{zz} = 1 + \left[\frac{\epsilon_h}{(\epsilon_{m,A} - \epsilon_h) f_{V,A}} - \frac{\beta_h^2 - k_z^2}{k_{p,A}^2} \right]^{-1} + \left[\frac{\epsilon_h}{(\epsilon_{m,B} - \epsilon_h) f_{V,B}} - \frac{\beta_h^2 - k_z^2}{k_{p,B}^2} \right]^{-1}. \quad (4)$$

For simplicity, in this paper we restrict our attention to the case wherein the metal can be described by a (lossless) Drude dispersion model such that $\epsilon_m(\omega) = \epsilon_0 (1 - \omega_m^2/\omega^2)$, in which ω_m the plasma frequency of the electron gas within the metal. In such a case, one can write $\frac{\epsilon_h}{(\epsilon_m - \epsilon_h) f_V} \approx -\frac{\epsilon_h}{\epsilon_0 f_V} \frac{\omega^2}{\omega_m^2} = -\frac{\beta_h^2}{f_V k_m^2}$ with $k_m = \omega_m \sqrt{\mu_0 \epsilon_0}$. Hence, after simple mathematical manipulations, it is found that

$$\epsilon_{zz}(\omega, k_z) = \epsilon_{zz,A}(\omega, k_z) + \epsilon_{zz,B}(\omega, k_z) - 1, \quad (5a)$$

$$\epsilon_{zz,l}(\omega, k_z) = 1 - \frac{k_{\text{eff},l}^2}{\beta_h^2 - k_z^2/n_l^2}, \quad (l = A, B), \quad (5b)$$

where $n_l^2 = 1 + \frac{k_{p,l}^2}{f_{V,l} k_m^2}$ is the so-called slow-wave factor¹⁸ that characterizes the plasmonic behavior of the wires, and $k_{\text{eff},l}^2 = k_{p,l}^2/n_l^2$ is the effective plasma wave number of each array that takes into account both the geometry of the cell and the permittivity of the metallic wires. In case the metal can be modeled as a perfect electrical conductor (PEC), the slow-wave factor is equal to unity (i.e., $n_l^2 = 1$), and therefore $k_{\text{eff},l}^2 = k_{p,l}^2$.

In Appendix A, we show that the macroscopic response (5) of the nested wire array can be understood in terms of an

equivalent drift-diffusion model such that two different species of carriers contribute to the current.

The characteristic equation for the photonic modes can be obtained if we substitute the permittivity tensor given by Eq. (3) into the Maxwell equations and calculate the plane wave solutions (eigenmodes) with a spatial variation of the form $e^{i\mathbf{k}\cdot\mathbf{r}}$, where $\mathbf{k} = \mathbf{k}_t + k_z \hat{\mathbf{z}}$ and $\mathbf{k}_t = k_x \hat{\mathbf{x}} + k_y \hat{\mathbf{y}}$. This yields the dispersion relation for transverse magnetic (TM)-polarized eigenwaves

$$k_z^2 = \beta_h^2 - \frac{k_x^2 + k_y^2}{1 - \frac{k_{\text{eff},A}^2}{\beta_h^2 - k_z^2/n_A^2} - \frac{k_{\text{eff},B}^2}{\beta_h^2 - k_z^2/n_B^2}}, \quad (6)$$

and $k_z^2 = \beta_h^2 - k_x^2 - k_y^2$ for the transverse electric (TE) polarized waves. For a given value of the transverse part of the wave vector, the dispersion relation (6) corresponds to a cubic equation that yields three different solutions, corresponding to three different propagating eigenmodes: two quasi-transverse electromagnetic (q-TEM) modes and a TM mode. We designate these qT1, qT2, and TM modes. This property contrasts with the standard wire medium that only supports two distinct extraordinary waves, the q-TEM mode and the TM mode.^{14,18} Each q-TEM mode is clearly associated with a different array of wires.^{14,18,24} This result can in principle be generalized, and we expect that in a material formed by N different wires arrays, such that the influence of each array on the others can be regarded as a macroscopic excitation, there will be N different propagating q-TEM waves.

III. SCATTERING PROBLEM AND ADDITIONAL BOUNDARY CONDITIONS

In what follows, we apply the theory developed in the previous section to characterize the scattering of electromagnetic waves by a finite thickness slab of the nested wire media of thickness h . A representative system geometry is sketched in Fig. 2. We consider that the incoming plane wave is TM polarized (magnetic field is along the y direction) so that the plane of incidence is the xoz plane. The angle of incidence is θ_{inc} , and the relevant field components are H_y , E_x , and E_z . This monochromatic incoming wave can excite plane waves in the wire medium with transverse wave

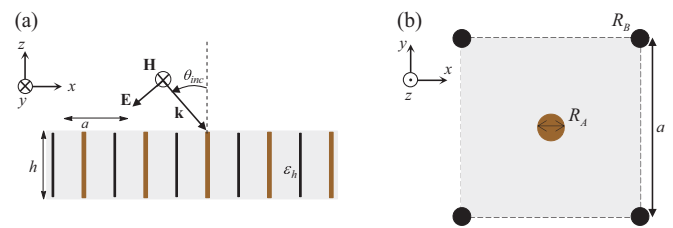


FIG. 2. (Color online) Geometry of the wire-medium slab formed by two nested sets of parallel wire arrays. (a) Side view: the cells are arranged in a periodic square lattice with period a . Both sets of wires are severed at the interfaces. The wires are embedded in a dielectric with permittivity ϵ_h and thickness h . The structure is illuminated by a TM-polarized plane wave with angle of incidence θ_{inc} . (b) Top view of the unit cell of a 2D lattice of a wire-medium slab with the one wire with radius R_A in the middle and another wire with radius R_B placed in the corners of the cell.

vector $\mathbf{k}_t = k_x \hat{\mathbf{x}} + k_y \hat{\mathbf{y}}$ such that $k_x = k_0 \sin \theta_{\text{inc}}$ and $k_y = 0$. Therefore, six plane waves can be excited in the wire medium: two counter-propagating waves (propagating along $+z$ and $-z$

directions, respectively) associated with each of the qT1, qT2, and TM modes. Thus, the magnetic field distribution in the whole space can be written as:

$$H_y(z, \omega) = e^{ik_x x} \frac{E^{\text{inc}}}{\eta_0} \begin{cases} (e^{\gamma_0 z} - R e^{-\gamma_0 z}) & z > 0 \\ C_1 e^{\gamma_{TM}(z+h)} + C_2 e^{-\gamma_{TM}(z+h)} + B_1 e^{\gamma_{qT2}(z+h)} + B_2 e^{-\gamma_{qT2}(z+h)} + A_1 e^{\gamma_{qT1}(z+h)} + A_2 e^{-\gamma_{qT1}(z+h)} & -h < z < 0, \\ T e^{\gamma_0(z+h)} & z < -h \end{cases} \quad (7a)$$

Using $\mathbf{E} = \frac{1}{-i\omega} [\bar{\boldsymbol{\varepsilon}}(\omega, -i \frac{d}{dz})]^{-1} \cdot \nabla \times \mathbf{H}$, it is found that the electric field satisfies

$$E_x(z, \omega) = e^{ik_x x} \frac{E^{\text{inc}}}{\eta_0} \frac{1}{i\omega \varepsilon_0} \begin{cases} \gamma_0 (e^{\gamma_0 z} + R e^{-\gamma_0 z}) & z > 0, \\ \frac{\varepsilon_0}{\varepsilon_h} \gamma_{TM} (C_1 e^{\gamma_{TM}(z+h)} - C_2 e^{-\gamma_{TM}(z+h)}) + \frac{\varepsilon_0}{\varepsilon_h} \gamma_{qT2} (B_1 e^{\gamma_{qT2}(z+h)} - B_2 e^{-\gamma_{qT2}(z+h)}) & -h < z < 0, \\ + \frac{\varepsilon_0}{\varepsilon_h} \gamma_{qT1} (A_1 e^{\gamma_{qT1}(z+h)} - A_2 e^{-\gamma_{qT1}(z+h)}) \\ \gamma_0 T e^{\gamma_0(z+h)} & z < -h \end{cases} \quad (7b)$$

$$E_z(z, \omega) = -e^{ik_x x} \frac{E^{\text{inc}}}{\eta_0} \frac{k_x}{\omega \varepsilon_0} \begin{cases} e^{\gamma_0 z} - R e^{-\gamma_0 z} & z > 0 \\ \frac{\varepsilon_0}{\varepsilon_{zz}^{TM}} (C_1 e^{\gamma_{TM}(z+h)} + C_2 e^{-\gamma_{TM}(z+h)}) + \frac{\varepsilon_0}{\varepsilon_{zz}^{qT2}} (B_1 e^{\gamma_{qT2}(z+h)} + B_2 e^{-\gamma_{qT2}(z+h)}) & -h < z < 0 \\ + \frac{\varepsilon_0}{\varepsilon_{zz}^{qT1}} (A_1 e^{\gamma_{qT1}(z+h)} + A_2 e^{-\gamma_{qT1}(z+h)}) \\ T e^{\gamma_0(z+h)} & z < -h \end{cases} \quad (7c)$$

In the above, $A_{1,2}$ and $B_{1,2}$ stand for the amplitude of the q-TEM modes, and $C_{1,2}$ stands for the amplitude of the TM modes in the nested wire media. The reflection and transmission coefficients are R and T , and $\gamma_0 = \sqrt{k_t^2 - \omega^2 \mu_0 \varepsilon_0}$ is the free-space propagation constant along the z direction. The propagation constants along z in the metamaterial ($\gamma^2 = -k_z^2$ with $\gamma = \gamma_{qT1}, \gamma_{qT2}, \gamma_{qTM}$) are obtained from the solution of the dispersion characteristic Eq. (6) with $\mathbf{k} = \mathbf{k}_t + k_z \hat{\mathbf{z}}$ and $\mathbf{k}_t = k_x \hat{\mathbf{x}}$. We put $\varepsilon_{zz}^{TM} = \varepsilon_h \varepsilon_{zz}(\omega, i \gamma_{TM})$, $\varepsilon_{zz}^{qT1} = \varepsilon_h \varepsilon_{zz}(\omega, i \gamma_{qT1})$, and $\varepsilon_{zz}^{qT2} = \varepsilon_h \varepsilon_{zz}(\omega, i \gamma_{qT2})$, where $\varepsilon_{zz}(\omega, k_z)$ is given by Eq. (5a).

To determine the unknowns $A_{1,2}$, $B_{1,2}$, $C_{1,2}$, R , and T , we need to impose suitable boundary conditions at the interfaces with the air regions. The boundary conditions depend on the manner in which the metallic wires are terminated at the interfaces. Here, we admit two possibilities: either the wires are cut at the interfaces, or alternatively, they are connected to square metallic patches. We suppose that all the wires in the same subarray are terminated in the same manner at the interface, but wires in different arrays can be terminated differently.

The classical boundary conditions establish a relation between the tangential components of the electric and magnetic fields at the interfaces. In the structure under consideration, the tangential electric field is continuous at the interface because there is no effective surface magnetization (or higher order surface multipole densities) at the interface. On the other hand, the tangential magnetic field may be discontinuous when an electric surface current is allowed. This can happen when one (or both) of the wire arrays are terminated with metallic patches. Therefore, we can write

$$[E_x]_{z=0, -h} = 0, \quad (8a)$$

$$[H_y]_{z=0, -h} = -Y_g E_x|_{z=0, -h}, \quad (8b)$$

where $[F]_{z=z_0} = F_{z=z_0^+} - F_{z=z_0^-}$ stands for the field discontinuity of F at the pertinent interface, and Y_g is the grid admittance, which relates the induced surface current with the tangential electric field. In the case in which both sets of wires are cut at the pertinent interface, $Y_g = 0$. An array of wires terminated with metallic patches separated by a gap g contributes to Y_g with the addend $Y_g = -i(\varepsilon_h + 1)(k_0 a / \eta_0 \pi) \log[\csc(\pi g / 2a)]$.¹⁸

It is well established that because of the strong spatial dispersion property, additional boundary conditions must be specified at the interfaces.^{19,30-33} Here, because we have two independent arrays of wires, two additional boundary conditions are required at each interface. Based on the ideas of Ref. 24, it is straightforward to formulate such boundary conditions.

Indeed, let us suppose first that the wires associated with a given subarray l are cut at the interface. Then, the microscopic current flowing on the metallic wires, I_l , should vanish at the interface. But, because the contribution \mathbf{P}_l of the subarray l to the total polarization vector is related to the current as $\mathbf{P}_l = \frac{1}{-i\omega} \frac{I_l}{a^2} \hat{\mathbf{z}}$, it follows that the boundary condition $I_l = 0$ at $z = z_0$ is equivalent to

$$\mathbf{P}_l \cdot \hat{\mathbf{z}}|_{z=z_0} = 0 \quad (\text{when subarray } l \text{ is cut at } z = z_0). \quad (8c)$$

On the other hand, let us suppose next that the wires of subarray l' are connected to metallic patches at the pertinent interface. For simplicity, we suppose that the metallic patches are large enough and the gap between the neighboring patches is small enough so that the effective patch capacitance¹⁹ $C_{\text{patch}} \rightarrow \infty$, and the average electric charge per unit of length of wire $\sigma_{l'} = \frac{1}{i\omega} \frac{dI_{l'}}{dz}$ may be assumed negligible at the connection point (as discussed in Refs. 19,31). In these circumstances, the boundary condition $\sigma_{l'} = 0$ must be enforced

at the interface, or equivalently:

$$\frac{d\mathbf{P}'}{dz} \cdot \hat{\mathbf{z}} \Big|_{z=z_0} = 0 \quad (\text{when subarray } l' \text{ is connected to large patches at } z = z_0). \quad (8d)$$

If we impose the boundary conditions (8a) and (8b) and the suitable ABC [either 8(c) or 8(d)] for the each of the subarrays ($l = A, B$) at the top and bottom interfaces, we obtain a set of eight linear equations for the eight unknowns. Note that from Eq. (2), we may rewrite Eqs. 8(c) and 8(d) as

$$\left[\varepsilon_{zz,l} \left(\omega, -i \frac{d}{dz} \right) - 1 \right] E_z \Big|_{z=z_0} = 0, \quad (8c')$$

$$\left[\varepsilon_{zz,l'} \left(\omega, -i \frac{d}{dz} \right) - 1 \right] \frac{dE_z}{dz} \Big|_{z=z_0} = 0, \quad (8d')$$

where $\varepsilon_{zz,l}$ is defined by Eq. (5b), and E_z is given by (7c).

In Appendix B we show that for lossless structures, these boundary conditions are consistent with the conservation of energy and with the continuity of the real part of the Poynting vector component normal to the interfaces.²²

It is worth mentioning that when the wires of the two subarrays are made of an ideal PEC material, the propagation constants associated with the two q-TEM modes become identical, such that $\gamma_{qT1} = \gamma_{qT2} = -i\beta_h$. As a consequence, it is clear that $\varepsilon_{zz}^{qT1} = \varepsilon_{zz}^{qT2} = \infty$, and hence the system of equations associated with the effective medium model becomes ill defined. This difficulty can be circumvented simply by slightly numerically perturbing the complex permittivity of the materials to lift the singularities. In general, one may need to adopt this perturbation approach when the propagation constants of the two q-TEM modes are identical. We checked both numerically and analytically that this approach leads to consistent results, independent of the considered perturbation.

IV. FANO RESONANCES

In order to demonstrate the validity of the proposed model and prove that the coupling of the wire arrays results in the emergence of Fano resonances, next we calculate the transmission and reflection properties of nested wire media with different structural parameters.

A. Nested wire media severed at both interfaces

To begin, we consider a configuration wherein the wires of both subarrays are cut at the interfaces (terminated in an open circuit). The wires are embedded in a dielectric medium with thickness h and permittivity ε_h . The wires of subarray A have radius R_A , whereas the wires of subarray B have radius R_B . The geometry is shown in Fig. 2.

In the first example, we consider that the slab has thickness $h = 3a$ and that the wires stand in air. The wire radii are $R_A = 0.05a$ and $R_B = 0.025a$ for each of the subarrays. Moreover, the metal is modeled as a PEC material, and the slab is illuminated by an incident TM-polarized plane wave with incidence angle $\theta_{\text{inc}} = 60^\circ$.

Because the two arrays are made of a PEC material, the system of equations of the effective medium model is ill

defined, as discussed previously. In practice this problem is solved by introducing a slight numerical perturbation in the slow-wave factor of the arrays such that $n_{A,B}^2 = 1 + \delta_{A,B}$, where $\delta_{A,B} \ll 1$. The reflection/transmission coefficients converge to the same result independent of the form of the perturbation when $\delta_{A,B} \rightarrow 0$. In panels (a) and (b) of Fig. 3, we compare the results obtained with our homogenization model and the ones obtained using the commercial full-wave electromagnetic simulator Microwave Studio.³⁴

One can see that there is a good agreement between the results obtained using the homogenization model and the full-wave simulations, indicating that our effective medium theory correctly describes the electromagnetic response of the nested wire media.

In the next example, we investigate the response of the structured slab when the permittivity of the metals is described by the Drude dispersion model. We consider that the wires of array B are made of a material such that $k_{m,B}a = 10.0$, which for a lattice period of $273\mu\text{m}$ is consistent with the plasma frequency of $0.92\text{ }\Omega\text{cm}$ p -type doped silicon.³⁵ On the other hand, we assume that the wires of array A have a plasma frequency that satisfies $k_{m,A}a = 19.5$, which corresponds to the plasma frequency of indium antimonide at 225 K .³⁶ As in the previous example, $h = 3a$, $R_A = 0.05a$, and $R_B = 0.025a$. A comparison between the results obtained with the homogenization model and full wave simulation is shown in panels (c) and (d) of Fig. 3. Apart from a frequency shift, the results show reasonable agreement, further validating our theory when the metallic wires are made of distinct materials.

Moreover, the plots reveal the presence of a sharp resonance in the transmission and reflection parameters near the normalized frequency $h\omega/c \approx 1.0$, whose asymmetric shape is consistent with a Fano-type resonance and differs markedly from the more common Lorentzian resonance.^{25,26} The physical origin of this resonance is related to the interference between a narrow quadrupole-type resonance, and a broad dipole-type resonance.²⁹ Indeed, short (subwavelength) wires behave to a first approximation as electric dipoles, such that their scattering strength typically increases with frequency. Hence, the scattering of the wire arrays is dominated by the strongly radiative collective dipolar mode resulting from the in-phase interference of the fields scattered by the two arrays, and in particular (for long wavelengths) the transmissivity of the structure tends to decrease as the frequency increases [see Figs. 3(a), 3(c)]. However, when the unit cell has two nested wires, the electromagnetic coupling of the nested wires may result in a narrow antibonding mode, such that the current in the wires of one of the subarrays flips sign over a narrow frequency range. At the frequency wherein the dipole moments of each array oscillate out of phase, the net dipole moment is zero, resulting in a subradiant mode, and in nearly 100% transmission of the incoming wave (the Fano resonance). For a frequency slightly smaller than that associated with the Fano resonance, the subarrays have a very strong dipolar response and the corresponding currents do not oscillate in opposition of phase, and this explains the dip in the transmission characteristic. This is illustrated in panel (a) of Fig. 4, where we show the phase and normalized amplitude of the z component of the polarization vector of each subarray of wires (defined by Eq. (2)) as a function of

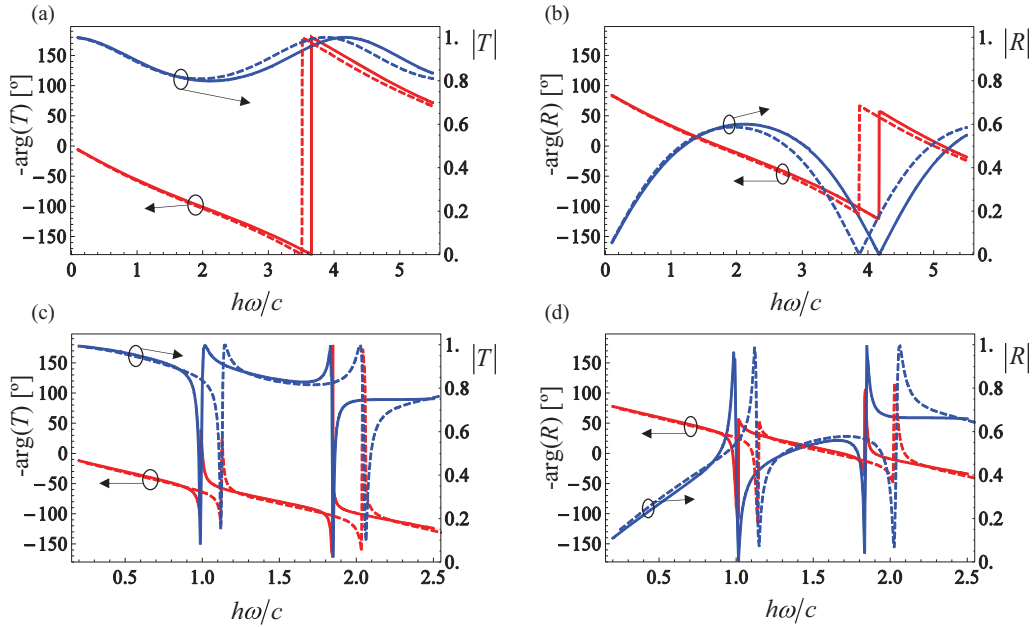


FIG. 3. (Color online) (a, b) Amplitude (blue curves) and phase (red curves) of the transmission and reflection coefficients for PEC wires and an incident TM-polarized wave with $\theta_{inc} = 60^\circ$ as a function of the normalized frequency $h\omega/c$. (c, d) Same as in the previous panels, but when the wires of subarrays A and B are made of metals such that for a lattice period of $a = 273 \mu\text{m}$, the normalized plasma frequencies satisfy $k_{m,A}a = 19.5$ and $k_{m,B}a = 10.0$. The solid lines represent the results calculated using the homogenization model, and the dashed lines represent the full wave results obtained with Microwave Studio.

frequency calculated at the midpoint of the wire-medium slab. In panel (b) of Fig. 4 we depict $P_{z,A}$ and $P_{z,B}$ inside the wire-medium slab at fixed frequencies. For the normalized frequency $h\omega/c \approx 1.0$, which corresponds to the peak of transmission at the Fano resonance, we see that not only are the polarization vectors out of phase, but they have nearly the same amplitude, confirming that the net polarization vector vanishes at the Fano resonance. For slightly different frequencies, the amplitudes of the polarization vectors are not the same, causing the dips in the amplitude transmission coefficient. Curiously, Fig. 4(a) shows that for frequencies smaller than $h\omega/c \approx 1.0$ this occurs because the amplitude of the polarization vector is larger in the subarray of wires with smaller radius, whereas

at frequencies slightly above $h\omega/c \approx 1.0$ the amplitude of the polarization vector is larger in the subarray of wires with larger radius.

Note that because the currents in the two wire arrays are out of phase, the narrow antibonding mode is related to quadrupole/magnetic resonances. Thus, at the Fano resonance the nested wires slab may mimic an array of magnetic dipoles that oscillate along the y direction. Moreover, because the Fano resonance results from the interaction of an electric-type resonance and magnetic-type resonance (more rigorously, a mix of magnetic and quadrupolar resonances), the nested wire medium may be roughly pictured as a material with an effective permittivity and an effective permeability that resonate at

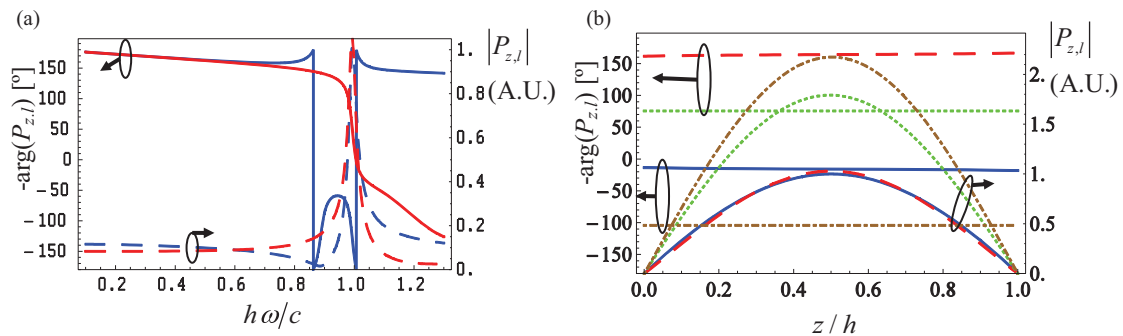


FIG. 4. (Color online) (a) Phase (solid curves) and normalized amplitude (dashed curves) of the z component of the macroscopic polarization vector of each subarray of wires at the middle of the slab as a function of the normalized frequency: polarization vector of submesh A (blue curves) and polarization vector of submesh B (red curves). The amplitude of the incident wave is constant. (b) Phase and normalized amplitude of the z component of the macroscopic polarization vector of each subarray of wires inside the wire-medium slab at $h\omega/c \approx 1.0$ (solid blue curves for submesh A and long dashed red curves for submesh B) and at $h\omega/c \approx 0.987$ (green dotted curves for submesh A and dot-dashed brown curves for submesh B).

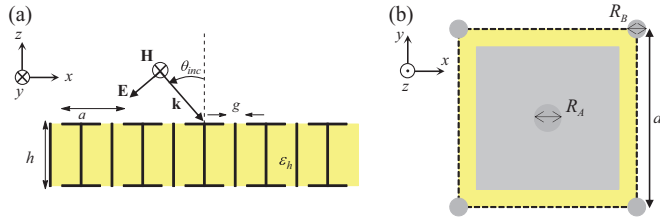


FIG. 5. (Color online) Similar to Fig. 2 but for a nested wire-medium slab terminated asymmetrically. (a) Side view: the cells are arranged in a periodic square lattice with period a , and one set of wires is terminated with patches. The separation between consecutive patches is g . (b) Top view of one cell of a 2D lattice of a wire-medium slab with one wire with radius R_A terminated with a patch and another wire with radius R_B placed at the corners of the cell and terminated with an open circuit.

nearby frequencies. In our system the Fano resonance results from the interaction of two different resonators (two different wire arrays), but there are examples in the literature wherein the Fano resonance is due to the interaction of different modes of the same resonator.^{29,37}

B. Nested wire media terminated asymmetrically

The emergence of the Fano resonance requires some asymmetry in the system, such that the antibonding resonance can be excited with a slow varying in space incoming wave. In the previous subsection, the asymmetry is provided by the different dielectric responses of the metals from which the wires are made of. Based on these ideas, one may expect that the Fano resonance can be more pronounced in systems with increased asymmetry.

To investigate this, next we calculate the transmission and reflection properties in a scenario wherein the wires of one of the subarrays (subarray B) are cut at both interfaces, and the wires of the other subarray (subarray A) are connected to metallic patches at both interfaces (Fig. 5). Hence, the two wire arrays are terminated asymmetrically. The spacing between adjacent patches is g , and the nested arrays are embedded in a dielectric with thickness h and permittivity ϵ_h . It should be mentioned that arrays of wires terminated with metallic

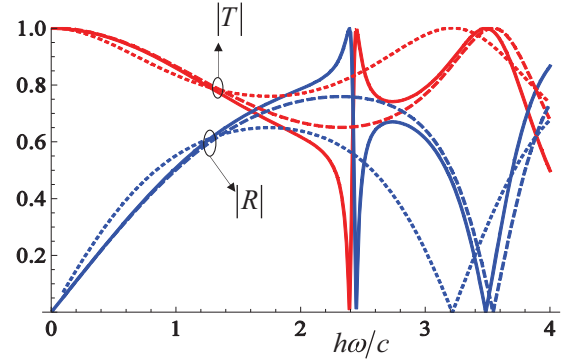


FIG. 7. (Color online) Amplitude of the transmission coefficient (red curves) and reflection coefficient (blue curves) of the nested wire-medium slab (solid curves), two-sided mushroom structure (dashed curves), and wire-medium slab (dotted curves) under the excitation of a TM-polarized wave with the angle of incidence $\theta_{inc} = 60^\circ$ as a function of the normalized frequency $h\omega/c$.

patches have been widely studied in the context of high-impedance surfaces in the so-called mushroom configuration (e.g., Refs. 6,16,17,38).

In the first example, it is supposed that the slab has thickness $h = 3a$ and the wires stand in a vacuum. The distance between adjacent patches is $g = 0.1a$, and the wire radius is $R_A = 0.05a$ and $R_B = 0.025a$ for each of the subarrays. The metal is modeled as a PEC material, and the slab is illuminated by an incident TM-polarized plane wave with incidence angle $\theta_{inc} = 60^\circ$. Because the wires are assumed to be PEC, it is again necessary to slightly perturb the slow-wave factors $n_{A,B}^2 = 1 + \delta_{A,B}$ with $\delta_{A,B} \approx 0$ to obtain a well-defined system of equations in the effective medium model. The computed results are shown in Fig. 6.

As expected, as the angle of incidence of the plane wave approaches 90° (Fig. 6(b) for the normalized frequency $h\omega/c = 1$), the structured slab tends to reflect all incident power because of the strong electromagnetic coupling between the incident waves and the wires.

The results in Fig. 6(a) show the signature of a sharp Fano resonance close to the normalized frequency $h\omega/c \approx 2.4$. In

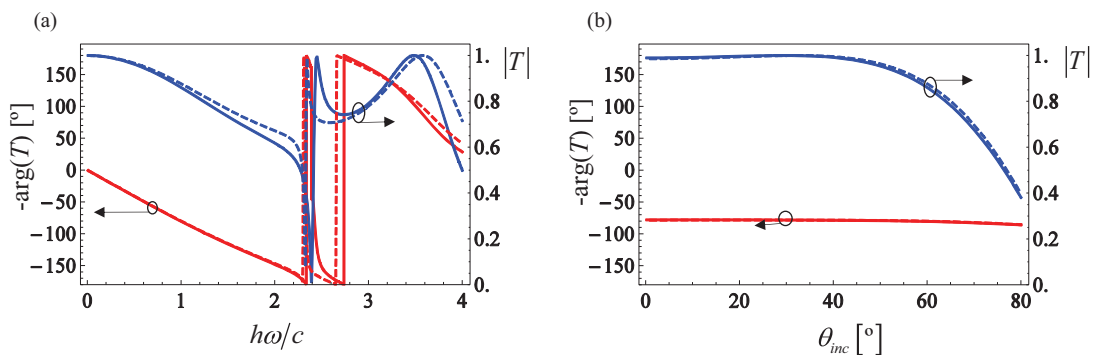


FIG. 6. (Color online) (a) Amplitude (blue curves) and phase (red curves) of the transmission coefficient under the excitation of a TM-polarized wave with the angle of incidence $\theta_{inc} = 60^\circ$ as a function of the normalized frequency $h\omega/c$. (b) Amplitude (blue curves) and phase (red curves) of the transmission coefficient for a fixed normalized frequency $h\omega/c = 1$ as a function of the incidence angle. The solid lines represent the results calculated using the homogenization model, and the dashed lines represent the results obtained with Microwave Studio.³⁴

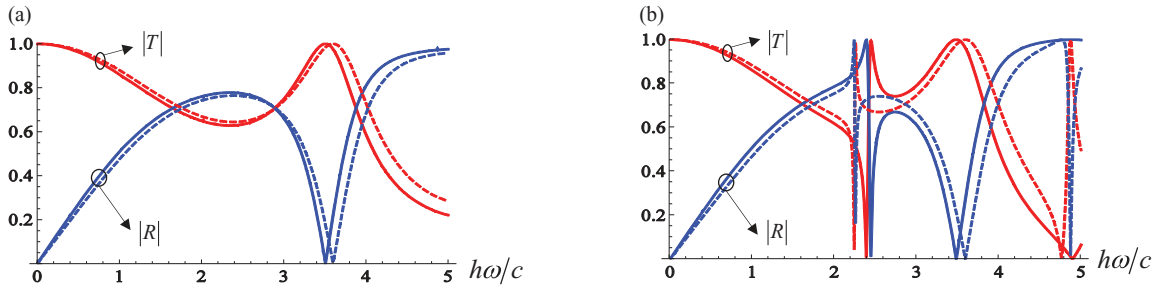


FIG. 8. (Color online) Amplitude of the transmission coefficient (red curves) and reflection coefficient (blue curves) as a function of the normalized frequency $h\omega/c$, obtained with the effective medium model (solid curves) and Microwave Studio (dashed curves). The wires of arrays A and B are made of metals such that for a lattice period of $a = 14 \mu\text{m}$, (a) $k_{m,A}a = 635.97$ and $k_{m,B}a = 1$ and (b) $k_{m,A}a = 635.97$ and $k_{m,B}a = 1043.9$. The slab thickness is $h = 3a$, and the angle of incidence is $\theta_{\text{inc}} = 60^\circ$.

contrast to the previous subsection, the Fano resonance can appear even for PEC wires due to the asymmetry in the termination of the wires.

To prove that the interaction of the two nested wire media is crucial for the emergence of the Fano resonance, we calculated the individual response of the arrays A and B in related scenarios. Figure 7 shows the transmission characteristics for a two-sided mushroom structure (only array A is present in the structure), for a wire-medium slab (only array B is present in the structure), and for the corresponding nested wire-medium slab. A sharp Fano resonance at the normalized frequency $h\omega/c \approx 2.4$ is revealed only in the latter configuration. These results were obtained based on the theories of previous works.^{14,19,30-33}

In order to investigate the effect of having metals with a dielectric response described by the Drude dispersion model, next we consider that the wires of array B are made of a metal such that $k_{m,B}a = 1.0$, which for a lattice period of $14 \mu\text{m}$ may be consistent with the plasma frequency of indium antimonide at 225 K.³⁶ The wires of array A are assumed to be made of silver, which for the same lattice period satisfies $k_{m,A}a = 635.97$.³⁹ In order to see the impact of using these materials

rather than a PEC material, we calculated the transmission characteristics of the metamaterial slab using our effective medium model [Fig. 8(a)], considering the same structural parameters as in the previous example. The results agree again quite well with full-wave simulations.

Comparing the results of panel (a) of Fig. 8 with panel (a) of Fig. 6, where PEC wires were considered in both arrays, it is seen that the resonant behavior near $h\omega/c \approx 2.4$ disappears, and the structure behaves more similar to a two-sided mushroom wire-medium slab as shown in the dashed curves of Fig. 7. The reason for this is simple: the plasma frequency of the material associated with the subarray B , $k_{m,B}a = 1$, is considerably smaller than the frequency $h\omega/c \approx 2.4$ where the Fano resonance originally occurred, and hence the material B does not have a typical metal-type response at that frequency and behaves closer to a transparent material.

Obviously if other metal is chosen with a large conductivity in the pertinent range of frequencies the Fano resonance will reappear. For instance, if the material of the wires of array B is aluminum, we have $k_{m,B}a = 1043.9$ ³⁹ for the same structural parameters as before. In this case the calculated transmission

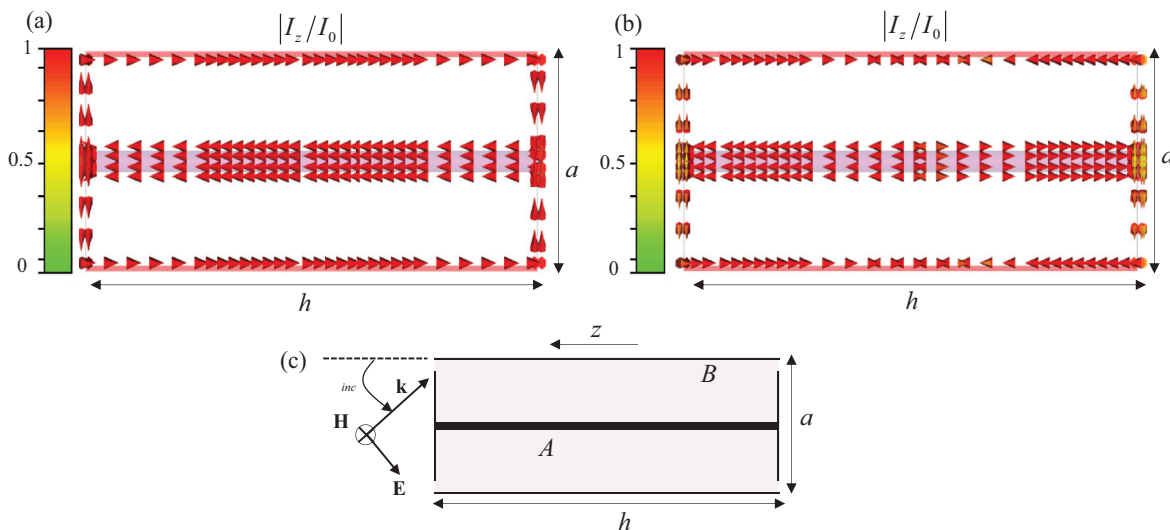


FIG. 9. (Color online) Normalized microscopic current density distribution in a unit cell of the nested wire-medium structure for the example of Fig. 8(b). The results are calculated for normalized frequencies (a) $h\omega/c = 2.25$ and (b) $h\omega/c = 3.6$. (c) Geometry of the unit cell.

and reflection parameters are as shown in Fig. 8(b), and the Fano resonance is evident.

To further confirm the nature of this resonance, in Fig. 9 we depict the normalized microscopic current density in the wires in a unit cell, for the structure associated with panel (b) of Fig. 8, at the normalized frequencies $h\omega/c = 2.25$ and at $h\omega/c = 3.6$, which correspond to the peaks of transmission calculated with Microwave Studio.³⁴ Consistent with Fig. 4, these results demonstrate that the narrowband Fano resonance [$h\omega/c = 2.25$; Fig. 9(a)] is rooted in the counterflow of microscopic currents in each set of wires, which originates a subradiant mode and the total transmission of the incoming wave. On the other hand, at the second resonance ($h\omega/c = 3.6$) the currents do not flow along a single direction in each wire, so the wires cannot be regarded as short dipoles.

V. CONCLUSION

In this paper we investigated the effective medium response of two nested arrays of parallel metallic wires. We studied the scattering of electromagnetic plane waves by a slab of the metamaterial, allowing the two arrays to be terminated in different manners. The results reveal that for wide incident angles the two arrays can be strongly coupled, and the currents in the two arrays may flow in opposite directions. This enables the interference of a narrow quadrupole-type resonance and a broad dipole-type resonance and results in Fano-type phenomena that can be useful in sensing.

ACKNOWLEDGMENTS

This work was funded by Fundação para Ciência e a Tecnologia under project PTDC/EEI-TEL/2764/2012. D.E.F. acknowledges support by Fundação para a Ciência e a Tecnologia, Programa Operacional Potencial Humano/POPH, and the cofinancing of Fundo Social Europeu under the fellowship SFRH/BD/70893/2010.

APPENDIX A: DRIFT-DIFFUSION MODEL FOR THE NESTED WIRE MEDIUM

In the following, we show that the spatially dispersive response of the nested wire medium can be understood in terms of a transport-based model and is related to diffusion effects. Moreover, we show that, compared to the case of a single wire array, the transport model for the nested wire medium is such that there are two inequivalent charge species (two independent channels) that contribute to the total current density. The starting point is a drift-diffusion model generalized for anisotropic media,

$$\begin{aligned} \mathbf{J}(\mathbf{r}) &= \boldsymbol{\sigma}_0 \cdot \mathbf{E}(\mathbf{r}) - \mathbf{D}_0 \cdot \nabla \rho(\mathbf{r}) \\ &= \boldsymbol{\sigma}_0 \cdot \mathbf{E}(\mathbf{r}) - \frac{1}{i\omega} \mathbf{D}_0 \cdot \nabla \nabla \cdot \mathbf{J}(\mathbf{r}), \end{aligned} \quad (\text{A1})$$

where $\boldsymbol{\sigma}_0 = \boldsymbol{\sigma}_0(\omega)$ and $\mathbf{D}_0 = \mathbf{D}_0(\omega)$ are the ‘‘local’’ conductivity and diffusion coefficient tensors that are assumed independent of position. If we assume conduction and diffusion only along the wire axis, then $\mathbf{D}_0 = \hat{\mathbf{z}}\hat{\mathbf{z}}D_z$ and $\boldsymbol{\sigma}_0 = \hat{\mathbf{z}}\hat{\mathbf{z}}\sigma_z$, so

that from (A1) we have $J_x = J_y = 0$ and

$$\left(1 + \frac{D_z}{i\omega} \frac{\partial^2}{\partial z^2}\right) J_z(\mathbf{r}) = \sigma_z E_z(\mathbf{r}).$$

Fourier transformation $z \leftrightarrow k_z$ leads to

$$\mathbf{J}(\boldsymbol{\rho}, k_z) = \hat{\mathbf{z}}\hat{\mathbf{z}} \frac{\sigma_z}{1 - \frac{D_z}{i\omega} k_z^2} \cdot \mathbf{E}(\boldsymbol{\rho}, k_z) = \boldsymbol{\sigma}(k_z) \cdot \mathbf{E}(\boldsymbol{\rho}, k_z), \quad (\text{A2})$$

where $\boldsymbol{\rho} = \hat{\mathbf{x}}x + \hat{\mathbf{y}}y$, and $\boldsymbol{\sigma}(k_z)$ is now a nonlocal conductivity tensor that accounts for both conduction and diffusion.

The response of the material is determined by the drift and diffusion currents associated with the free carriers and by the bound-charge contribution. In the following we will assume that the polarization response is local but anisotropic, governed by the permittivity tensor $\boldsymbol{\varepsilon}_b$. From Ampere’s law,

$$\nabla_{k_z} \times \mathbf{H}(\boldsymbol{\rho}, k_z) = -i\omega \left(\boldsymbol{\varepsilon}_b + i \frac{1}{\omega} \boldsymbol{\sigma}(k_z) \right) \cdot \mathbf{E}(\boldsymbol{\rho}), \quad (\text{A3})$$

where $\nabla_{k_z} = \hat{\mathbf{x}}\partial/\partial x + \hat{\mathbf{y}}\partial/\partial y + \hat{\mathbf{z}}ik_z$, we obtain the combined permittivity

$$\bar{\boldsymbol{\varepsilon}}(\omega, k_z) = \boldsymbol{\varepsilon}_b + \hat{\mathbf{z}}\hat{\mathbf{z}} \frac{\sigma_z}{-i\omega + D_z k_z^2}.$$

If we compare this response with the macroscopic response of the standard wire medium (1), when the metal dielectric function is described by the Drude model, we see that $\boldsymbol{\varepsilon}_b = \bar{\mathbf{I}}\boldsymbol{\varepsilon}_h$ and

$$\sigma_z = i\omega\varepsilon_h \frac{k_{\text{ef}}^2}{\beta_h^2} = \frac{i\omega\varepsilon_h}{\beta_h^2} \left(\frac{1}{k_p^2} + \frac{1}{k_m^2 f_V} \right)^{-1} = D_z \varepsilon_h k_p^2 \quad (\text{A4})$$

$$D_z = \frac{i\omega}{\beta_h^2 n_A^2} = \frac{i\omega}{\beta_h^2 k_p^2} \left(\frac{1}{k_p^2} + \frac{1}{k_m^2 f_V} \right)^{-1}. \quad (\text{A5})$$

On the other hand, when the metal is described by a constant conductivity model such that $\varepsilon_m \approx \sigma_m/(-i\omega)$ we find from Eq. (1) that the corresponding drift-diffusion model parameters are

$$\sigma_z \approx \frac{k_p^2/\mu_0}{-i\omega + \tau_{WM}^{-1}}, \quad D_z \approx \frac{v_h^2}{-i\omega + \tau_{WM}^{-1}}, \quad (\text{A6})$$

where $\tau_{WM} = \sigma_m f_V \mu_0 / k_p^2$ is an equivalent relaxation time and $v_h = 1/\sqrt{\mu_0 \varepsilon_h}$ is the phase velocity in the host medium. Thus, in general, the uniaxial wire-medium dielectric function can be written in terms of an effective conductivity and diffusion model as

$$\bar{\boldsymbol{\varepsilon}}(\omega, k_z) = \bar{\mathbf{I}}\boldsymbol{\varepsilon}_h + \hat{\mathbf{z}}\hat{\mathbf{z}} \frac{\sigma_z}{-i\omega + D_z k_z^2}. \quad (\text{A7})$$

As discussed in Ref. 24, for natural nonlocal materials such as semiconductors, when two charge species A and B (e.g., electrons and ions) are present, the spatial transform permittivity has the form

$$\bar{\boldsymbol{\varepsilon}}(\omega, \mathbf{k}) = \boldsymbol{\varepsilon}_h + i \frac{1}{\omega} \boldsymbol{\sigma}_A(\mathbf{k}, \omega) + i \frac{1}{\omega} \boldsymbol{\sigma}_B(\mathbf{k}, \omega), \quad (\text{A8})$$

where the interactions among charge species comes from the electric field \mathbf{E} , being the self-consistent field. An isotropic triple-wire array system leads to the same form for the

permittivity,²⁴ and for the two nested wire arrays considered, we have:

$$\bar{\epsilon}(\omega, \mathbf{k}) = \epsilon_h + \hat{\mathbf{z}}\hat{\mathbf{z}} \frac{\sigma_{z,A}}{-i\omega + D_{z,A}k_z^2} + \hat{\mathbf{z}}\hat{\mathbf{z}} \frac{\sigma_{z,B}}{-i\omega + D_{z,B}k_z^2}, \quad (\text{A9})$$

where the l th current component satisfies

$$\left(1 + \frac{D_{z,l}}{i\omega} \frac{\partial^2}{\partial z^2}\right) J_{z,l}(\mathbf{r}) = \sigma_{z,l} E_z(\mathbf{r}), \quad (\text{A10})$$

wherein E_z is the z component of the self-consistent field associated with $J_{z,A}$, $J_{z,B}$, and bound charge polarization current $\mathbf{J}_p = -i\omega(\epsilon_h - \epsilon_0)\mathbf{E}$.

The drift-diffusion approach has two important assets. One is that it allows the definition of a Debye length for the l th wire system (in this case along the wire axis),

$$k_{D,l}^2 = \frac{-i\omega\epsilon_h + \sigma_l}{D_l\epsilon_h}, \quad (\text{A11})$$

that gives a measure of charge screening, as it does for natural materials. It is found that the Debye length for wire media is much larger than that for natural materials,²⁴ attesting to the strength of nonlocal effects. The second benefit of the drift-diffusion model is for three-dimensional problems. Solving equations of the form $\mathbf{J}(\mathbf{r}) = \int \boldsymbol{\sigma}(\mathbf{r} - \mathbf{r}') \cdot \mathbf{E}(\mathbf{r}') d^3\mathbf{r}'$ involves at least sixfold convolution integrals (three from the convolution of $\boldsymbol{\sigma}$ and \mathbf{E} , and three relating \mathbf{E} to current, $\mathbf{E}(\mathbf{r}) = \int \bar{\mathbf{G}}(\mathbf{r} - \mathbf{r}') \cdot \mathbf{J}(\mathbf{r}') d^3\mathbf{r}'$, and more if $\boldsymbol{\sigma}(\mathbf{r})$ is not determined in closed form. However, the drift-diffusion form (A10) involves only threefold integrals relating \mathbf{E} and \mathbf{J} by Green's dyadic $\bar{\mathbf{G}}$. This has been shown to lead to a practical way to model scattering from three-dimensional wire media.^{40,41} Double-nested wire arrays can be modeled in the same manner, although that topic is beyond the scope of the present work.

APPENDIX B: ENERGY CONSERVATION AND POYNTING VECTOR DEFINITION IN NESTED WIRE MEDIA

The definition of the Poynting vector in the standard uniaxial wire medium has been studied in a previous work, where it was demonstrated that it should be written not only in terms of the macroscopic electromagnetic field, but also in terms of the so-called additional potential φ and of the current that travels along the wires I (Refs. 19,42). Specifically, one has⁴²

$$\mathbf{S}_{\text{av}} = \frac{1}{2} \text{Re} \left\{ \mathbf{E} \times \mathbf{H}^* + \frac{\varphi I^*}{A_c} \hat{\mathbf{z}} \right\}, \quad (\text{B1})$$

where $A_c = a^2$. To generalize this result and formulate an energy conservation theorem for the wire medium formed by nested sets of wires, we start by writing the Maxwell equations in the time domain as

$$\nabla \times \mathbf{E} = -\mu_0 \frac{\partial \mathbf{H}}{\partial t}, \quad (\text{B2})$$

$$\nabla \times \mathbf{H} = \epsilon_h \frac{\partial \mathbf{E}}{\partial t} + \frac{\mathbf{I}_{\text{tot}}}{A_c} \hat{\mathbf{z}} + \mathbf{J}_{\text{ext}}, \quad (\text{B3})$$

where \mathbf{J}_{ext} is an hypothetical macroscopic (external) current density and the total conduction current is given by summation of the two currents along the wires: $\mathbf{I}_{\text{tot}} = I_{\text{tot}} \hat{\mathbf{z}} = \sum_l I_l \hat{\mathbf{z}}$. In our case, each array of wires is characterized by an additional

potential and microscopic current, which in the time domain satisfy (see Ref. 42 for a related result):

$$\frac{\partial I_l}{\partial z} = -C_l \frac{\partial \varphi_l}{\partial t}, \quad (\text{B4})$$

$$\frac{\partial \varphi_l}{\partial z} = -(L_l + L_{w,l}) \frac{\partial I_l}{\partial t} - R_{w,l} I_l + E_z, \quad (\text{B5})$$

with $l = A, B$, where $Z_{w,l} = -i\omega L_{w,l} + R_{w,l} = -1/i\omega\pi R_l^2 \epsilon_0 (\epsilon_{m,l} - 1)$ is the self-impedance of the wires,¹⁸ $C_l = 2\pi\epsilon_0 / \log[a^2/4R_l(a - R_l)]$ is the effective capacitance per unit of length (p.u.l.) of wire,¹⁸ and $L_l = \log[a^2/4R_l(a - R_l)]\mu_0/2\pi$ is the effective p.u.l. inductance¹⁸ in each wire array.

Following a procedure analogous to that reported in Ref. 42 it is possible to calculate the instantaneous macroscopic Poynting vector \mathbf{S} in the wire medium, the instantaneous density of stored energy W , the instantaneous density of power transferred from the sources to the medium P_{ext} , and the instantaneous power loss density P_{loss} :

$$\mathbf{S} = \mathbf{E} \times \mathbf{H} + \sum_l \frac{\varphi_l I_l}{A_{\text{cell}}} \hat{\mathbf{z}}, \quad (\text{B6})$$

$$W = \sum_l \left(\frac{(L_l + L_{w,l})}{2A_c} I_l^2 + \frac{C_l \varphi_l^2}{2A_c} \right) + \frac{\mu_0}{2} \mathbf{H}^2 + \frac{\epsilon_h}{2} \mathbf{E}^2, \quad (\text{B7})$$

$$P_{\text{loss}} = \sum_l R_{w,l} I_l^2, \quad (\text{B8})$$

$$P_{\text{ext}} = \mathbf{J}_{\text{ext}} \cdot \mathbf{E}, \quad (\text{B9})$$

In the case of a time-harmonic electromagnetic field with frequency of oscillation ω , the time-averaged Poynting vector can be expressed as

$$\mathbf{S}_{\text{av}} = \frac{1}{2} \text{Re} \left\{ \mathbf{E} \times \mathbf{H}^* + \sum_l \frac{\varphi_l I_l^*}{A_c} \hat{\mathbf{z}} \right\}. \quad (\text{B10})$$

This formula extends the result of Ref. 42 and can be further generalized to other systems of metallic wires that interact with one another as macroscopic excitations.

Next, we demonstrate that in the lossless case, the boundary conditions proposed in Sec. III guarantee the continuity of the real part of the z component of the Poynting vector at a generic interface, and hence the conservation of energy. Let us consider, for instance, the top interface of a wire-medium slab corresponding to the plane $z = 0$. At this plane the continuity of S_z is equivalent to

$$\begin{aligned} & \text{Re} \left\{ \frac{1}{2} \left(E_{x,WM} H_{y,WM}^* |_{z=0} + \sum_l \frac{\varphi_l I_{l,z}^*}{A_c} \Big|_{z=0} \right) \right\} \\ &= \text{Re} \left\{ \frac{1}{2} E_{x,\text{air}} H_{y,\text{air}}^* |_{z=0} \right\}, \end{aligned} \quad (\text{B11})$$

where the subscripts *WM* and *air* indicate at which side of the interface the fields are evaluated. This equation is equivalent to

$$\text{Re} \{ E_{x,WM} (H_{y,\text{air}}^* - H_{y,WM}^*) |_{z=0} \} = \text{Re} \left\{ \sum_l \frac{\varphi_l I_{l,z}^*}{A_c} \Big|_{z=0} \right\}. \quad (\text{B12})$$

We can easily identify $(H_{y,\text{air}}^* - H_{y,WM}^*)|_{z=0} = [H_y^*]_{z=0}$ as $(-Y_g E_x|_{z=0})^*$ using the boundary condition (8b). In the lossless case, the grid admittance is a pure imaginary number, and hence,

$$\text{Re}\{E_{x,WM}(H_{y,\text{air}}^* - H_{y,WM}^*)|_{z=0}\} = 0. \quad (\text{B13})$$

So the continuity of S_z reduces to

$$\text{Re}\left\{\sum_l \frac{\varphi_l I_{l,z}^*}{A_c} \Big|_{z=0}\right\} = 0. \quad (\text{B14})$$

On the other hand, in general, it is possible to write that at the interface,¹⁹

$$\varphi_l = \frac{I_l}{-i\omega C_{\text{end},l}} \quad (l = A, B), \quad (\text{B15})$$

where $C_{\text{end},l}$ depends on the manner that the metallic wires are terminated at the interface. For example, for cut wires, $C_{\text{end}} \approx C_{\text{tip}} \approx 0$, whereas for wires connected to large metallic patches, $C_{\text{end}} \approx C_{\text{patch}} \approx \infty$ (Ref. 19). In any case, provided C_{end} is a real number, we find that:

$$\begin{aligned} & \text{Re}\left\{\sum_l \frac{\varphi_l I_{l,z}^*}{A_c} \Big|_{z=0}\right\} \\ &= \text{Re}\left\{\frac{I_A}{-i\omega C_{\text{end},A}} I_A^* + \frac{I_B}{-i\omega C_{\text{end},B}} I_B^* \Big|_{z=0}\right\} = 0 \end{aligned} \quad (\text{B16})$$

and therefore Eq. (B15) is indeed satisfied, as we wanted to prove.

*dfernandes@co.it.pt

†stas@co.it.pt

‡george@uwm.edu

§Author to whom correspondence should be addressed: mario.silveirinha@co.it.pt

¹J. B. Pendry, A. J. Holden, W. J. Stewart, and I. Youngs, *Phys. Rev. Lett.* **76**, 4773 (1996).

²S. I. Maslovski, S. A. Tretyakov, and P. A. Belov, *Microwave Opt. Tech. Lett.* **35**, 47 (2002).

³D. R. Smith and D. Schurig, *Phys. Rev. Lett.* **90**, 077405 (2003).

⁴J. Yao, Z. Liu, Y. Liu, Y. Wang, C. Sun, G. Bartal, A. M. Stacy, and X. Zhang, *Science* **321**, 930 (2008).

⁵M. G. Silveirinha, *Phys. Rev. B* **79**, 153109 (2009).

⁶S. A. Tretyakov and S. I. Maslovski, *Microwave Opt. Tech. Lett.* **38**, 175 (2003).

⁷M. G. Silveirinha, *Phys. Rev. Lett.* **102**, 193903 (2009).

⁸P. A. Belov, G. K. Palikaras, Y. Zhao, A. Rahman, C. R. Simovski, Y. Hao, and C. Parini, *Appl. Phys. Lett.* **97**, 191905 (2010).

⁹T. A. Morgado, J. S. Marcos, M. G. Silveirinha, and S. I. Maslovski, *Appl. Phys. Lett.* **97**, 144102 (2010).

¹⁰S. Paulotto, P. Baccarelli, P. Burghignoli, G. Lovat, G. W. Hanson, and A. B. Yakovlev, *IEEE Trans. Microwave Theory Tech.* **58**, 1807 (2010).

¹¹T. A. Morgado, J. S. Marcos, M. G. Silveirinha, and S. I. Maslovski, *Phys. Rev. Lett.* **107**, 063903 (2011).

¹²J. T. Costa and M. G. Silveirinha, *Opt. Express* **20**, 13915 (2012).

¹³P. A. Belov, R. Marques, S. I. Maslovski, I. S. Nefedov, M. Silveirinha, C. R. Simovski, and S. A. Tretyakov, *Phys. Rev. B* **67**, 113103 (2003).

¹⁴M. G. Silveirinha, *Phys. Rev. E* **73**, 046612 (2006).

¹⁵A. Demetriadou and J. B. Pendry, *Phys. Condens. Matter* **20**, 295222 (2008).

¹⁶O. Luukkonen, M. G. Silveirinha, A. B. Yakovlev, C. R. Simovski, I. S. Nefedov, and S. A. Tretyakov, *IEEE Trans. Microwave Theory Tech.* **57**, 2692 (2009).

¹⁷A. B. Yakovlev, M. G. Silveirinha, O. Luukkonen, C. R. Simovski, I. S. Nefedov, and S. A. Tretyakov, *IEEE Trans. Microwave Theory Tech.* **57**, 2700 (2009).

¹⁸S. I. Maslovski and M. G. Silveirinha, *Phys. Rev. B* **80**, 245101 (2009).

¹⁹S. I. Maslovski, T. A. Morgado, M. G. Silveirinha, C. S. R. Kaipa, and A. B. Yakovlev, *New J. Phys.* **12**, 113047 (2010).

²⁰J. Shin, J.-T. Shen, and S. Fan, *Phys. Rev. B* **76**, 113101 (2007).

²¹M. G. Silveirinha and C. A. Fernandes, *Phys. Rev. B* **78**, 033108 (2008).

²²M. G. Silveirinha, *New J. Phys.* **11**, 113016 (2009).

²³M. G. Silveirinha, *Phys. Rev. B* **79**, 035118 (2009).

²⁴G. W. Hanson, E. Forati, and M. G. Silveirinha, *IEEE Trans. Antennas Propag.* **60**, 4219 (2012).

²⁵U. Fano, *Phys. Rev.* **124**, 1866 (1961).

²⁶A. E. Miroshnickenko, S. Flach, and Y. S. Kivshar, *Rev. Mod. Phys.* **82**, 2257 (2010).

²⁷V. A. Fedotov, M. Rose, S. L. Prosvirnin, N. Papasimakis, and N. I. Zheludev, *Phys. Rev. Lett.* **99**, 147401 (2007).

²⁸N. A. Mirin, K. Bao, and P. Nordlander, *J. Phys. Chem. A* **113**, 4028 (2009).

²⁹B. Luk'yanchuk, N. I. Zheludev, S. A. Maier, N. J. Halas, P. Nordlander, H. Giessen, and C. T. Chong, *Nat. Mater.* **9**, 707 (2010).

³⁰M. G. Silveirinha, *IEEE Trans. Antennas Propag.* **54**, 1766 (2006).

³¹M. G. Silveirinha, C. A. Fernandes, and J. R. Costa, *New J. Phys.* **10**, 053011 (2008).

³²C. S. R. Kaipa, A. B. Yakovlev, S. I. Maslovski, and M. G. Silveirinha, *Phys. Rev. B* **84**, 165135 (2011).

³³C. S. R. Kaipa, A. B. Yakovlev, S. I. Maslovski, and M. G. Silveirinha, *IEEE Antennas and Wireless Propag. Lett.* **10**, 1503 (2011).

³⁴CST GmbH 2013 CST Microwave Studio, <http://www.cst.com>.

³⁵M. van Exter and D. Grischkowsky, *Appl. Phys. Lett.* **56**, 1694 (1990).

³⁶J. G. Rivas, C. Janke, P. Bolivar, and H. Kurz, *Opt. Express* **13**, 847 (2005).

³⁷M. Sarrazin, J.-P. Vigneron, and J.-M. Vigoureux, *Phys. Rev. B* **67**, 085415 (2003).

³⁸F. Yang and Y. Rahmat-Samii, *Microwave and Opt. Tech. Lett.* **41**, 6 (2004).

- ³⁹M. A. Ordal, R. J. Bell, R. W. Alexander, Jr., L. L. Long, and M. R. Query, *Appl. Opt.* **24**, 4493 (1985).
- ⁴⁰E. Forati and G. W. Hanson, "Interaction of electromagnetic waves and three-dimensional wire media," *IEEE Trans. Antennas Propagat.* (to be published).
- ⁴¹E. Forati and G. W. Hanson, "A transport model for homogenized uniaxial wire media: three dimensional scattering problems and homogenized model limits" (unpublished).
- ⁴²M. G. Silveirinha and S. I. Maslovski, *Phys. Rev. B* **85**, 155125 (2012).